

### 33B.0 In Situ Studies of Strain Rate Effects on Phase Transformations and Microstructural Evolution in Multiple Principle Element Alloys

John Copley (Mines)

Faculty: Amy Clarke (Mines)

Other Participants: Y. Guo (Mines), J. Klemm-Toole (Mines), F.G. Coury (UFSCar)

Industrial Mentor: TBD

This project initiated in Fall 2017 and is supported by the Office of Naval Research. The research performed during this project will serve as the basis for an M.S./Ph.D. thesis for John Copley.

#### 33B.1 Project Overview and Industrial Relevance

Multiple Principle Element Alloys (MPEAs) have gained recent interest, as they represent a relatively unexplored alloy design space, being centered in, rather than at, the corners of ternary, quaternary and quinary phase diagrams [33B.1]. Most conventional alloys have only one or two elements in significant concentrations, and therefore relatively fewer possible combinations as compared to MPEAs. Some MPEAs, especially those from the CoCrNi family, have the potential to exhibit transformation and twinning induced plasticity (TRIP and TWIP respectively), where plastic deformation is accommodated by shifts in the stacking sequence of specific atomic planes, in addition to dislocation motion [33B.2]. The combination of TRIP/TWIP, in addition to dislocation motion and multiplication, results in high work hardening rates, as the boundaries of transformation product and twin interfaces act as barriers to dislocation motion [33B.3]. Materials with high work hardening rates are, in turn, associated with increased ductility and strength when compared to materials with otherwise similar properties and lower work hardening rates, as predicted by the Considère instability criterion  $\sigma = d\sigma/d\varepsilon$ . The influence of strain hardening rate on ultimate tensile strength and uniform elongation in a tensile test is illustrated in **Figure 33B.1** Increasing the ductility of a material without a corresponding decrease in strength increases the area under the stress-strain curve. A larger area under a stress strain curve indicates a larger specific plastic work to fracture, which is one measure of toughness.

Materials with high toughness are useful in engineering applications, as they are able to absorb higher amounts of energy before failure. High energy absorption is especially useful for blast resistance, which is the primary focus of this project. Increased energy absorption/toughness reduces the required amount of armor for similar protection against explosive reactions. Outside of blast resistance, the extended ductility of TRIP/TWIP materials improves their formability, allowing them to be worked into complex geometries that require higher strains. Studies of the effects of strain rate and state, as well as phase stability and deformation mechanisms, on the deformation behavior and microstructural evolution of MPEAs will enable alloy design for specific applications. Furthermore, better fundamental understanding of TRIP/TWIP behavior may have extensions to more commonly used advanced high strength steels that exhibit TRIP/TWIP behavior, in addition to metastable  $\beta$ -titanium alloys – a complementary project underway in CANFSA.

#### 33B.2 Previous Work

A review of the existing literature reveals a few families of MPEAs that have received much attention. The Cantor Alloy, an equi-atomic CoCrFeMnNi FCC solid solution, has been shown to be the toughest true high-entropy-alloy (with an entropy of mixing greater than 1.5R) [33B.1]. Work by George *et al.* has shown that the equi-atomic CoCrNi medium entropy alloy has superior strength and ductility as compared to the Cantor alloy [33B.4]. Work on CoCrNi equi-atomic alloys has shown the formation of nano-twins during deformation resulting in enhanced strength and toughness at cryogenic temperatures when twinning becomes more prominent [33B.5]. As compared to other material systems, CoCrNi alloys have promising combinations of strength and ductility. Accordingly, the CoCrNi ternary system was selected as the initial system of interest in this work.

Evidence of TRIP behavior in a  $\text{Co}_{0.55}\text{Cr}_{0.40}\text{Ni}_{0.05}$  MPEA was seen following cold rolling to 25% by Dr. Francisco Coury during his PhD work. Initial microstructural characterization of the cold rolled material showed the presence of both deformation twins and transformation product. Thermo-Calc modeling of  $T_0$ , the temperature at which two phases have the same free energy and the same composition, indicated a high  $T_0$  (above 900°C) for this alloy. A high  $T_0$  temperature indicates that a diffusionless transformation (and the possibility of TRIP) can occur at elevated temperatures. A 2 kg ingot of the  $\text{Co}_{0.55}\text{Cr}_{0.40}\text{Ni}_{0.05}$  alloy was prepared via spray-forming at the Federal University of Sao Carlos (UFSCar), in Brazil by Dr. Guilherme Zepon.

### 33B.3 Recent Progress

The  $\text{Co}_{0.55}\text{Cr}_{0.40}\text{Ni}_{0.05}$  material spray formed at UFSCar was used in in-situ synchrotron x-ray diffraction (XRD)/thermo-mechanical experiments conducted by Dr. Francisco Coury at the Brazilian Light Source (LNLS). Recent work has focused on processing the data from LNLS and preparing a journal article based on these experiments. The XRD/thermo-mechanical tests were conducted using quasi-static strain rates at a variety of temperatures, ranging from -100°C to 900°C. The XRD data show transformation of the FCC phase to HCP during deformation in all tests conducted from -100°C to 450°C. Data showing the appearance of an HCP phase in the XRD data with increasing strain is included as **Figure 33B.2**. For temperatures above 450°C, the XRD data does not show evidence of the HCP phase, indicating the deformation-induced transformation is suppressed, as indicated in **Figure 33B.3**. The stress-strain data from tensile tests conducted at temperatures between -100 °C – 750 °C are shown in **Figure 33B.4**. Premature failure may have occurred in these samples, due to defects/pores that formed during the spray forming process. Spray forming was initially used to allow for larger scale production of MPEAs compared to arc melting. However, the spray forming process is not fully optimized to produce low porosity samples. Also included are plots of instantaneous work hardening exponents as a function of strain, as shown in **Figure 33B.5**. There is a difference in the response of the instantaneous work hardening exponent to strain between the low temperature tests where transformation occurs and the high temperature tests where XRD data suggests no transformation occurs. The changes in instantaneous strain hardening exponent with plastic strain, combined with XRD data, suggest there is a difference in deformation mechanism, consistent with the suppression of TRIP behavior at high temperature. This work was presented as a poster entitled “TRIP behavior in the  $\text{Co}_{0.55}\text{Cr}_{0.40}\text{Ni}_{0.05}$  MPEA” at a recent Office of Naval Research (ONR) MPEA workshop hosted at the University of California-Santa Barbara, in January 2019.

This project, as well as its compliment focusing on metastable  $\beta$ -titanium alloys (Project #33A), were awarded beam time from a general user proposal at the Advanced Photon Source (APS) at Argonne National Laboratory. In-situ XRD and Kolsky bar (Split-Hopkinson bar) compression and tension experiments were conducted at the APS 32-ID-B beamline, with the goal of observing x-ray diffraction evolution due to TRIP behavior at high strain rates (on the order of  $10^3 \text{ s}^{-1}$ ) and dynamic response during deformation. Samples of nominal compositions:  $\text{Co}_{0.50}\text{Cr}_{0.40}\text{Ni}_{0.10}$ ,  $\text{Co}_{0.40}\text{Cr}_{0.40}\text{Ni}_{0.20}$ ,  $\text{Co}_{0.30}\text{Cr}_{0.40}\text{Ni}_{0.30}$  (along the  $\text{Co}_{(0.60-x)}\text{Cr}_{0.40}\text{Ni}_x$  line) and the equi-atomic  $\text{CoCrNi}$ , were produced by arc melting. Tensile specimens were tested at one strain rate and compression samples were tested at two strain rates. Preliminary analysis of the XRD data shows the evolution of a few individual spots to diffuse rings upon deformation, indicating crystallite refinement possibly from the formation of deformation twins. Post-mortem characterization is underway.

### 33B.4 Plans for Next Reporting Period

Key for the next reporting period will be the analysis of the data collected at the APS to generate movies of deformation, XRD, and stress-strain plots. Post mortem electron microscopy of tested samples, especially energy dispersive x-ray spectroscopy (EDS), will be performed to assess the chemical homogeneity of the arc melted buttons. Post mortem XRD analysis will provide data with a better signal to noise ratio and could be used for more accurate estimations of phase fractions post deformation. Additional time at APS has been requested for an upcoming cycle. If awarded, additional buttons will be produced and efforts to reduce the

grain size and thickness of the samples will be taken, in order to result in a greater degree of x-ray transmission through samples that contain multiple grains within the gauge volume of the specimens.

Other experiments will be performed to confirm and correlate the results obtained at APS, specifically characterization of the thermal effects on TRIP/TWIP behavior and mechanical properties. In-situ dynamic transmission electron microscopy (DTEM) experiments using a piezo-electric stage that allows imaging at high ( $10^4 \text{ sec}^{-1}$ ) strain rates, while capturing images at higher frame rates than traditional TEM imaging, may also be pursued in this project.

### **33B.5 References**

- [33B.1] D.B. Miracle, J.D. Miller, O.N. Senkov, C. Woodward, M.D. Uchic, J. Tiley, Exploration and Development of High Entropy Alloys for Structural Applications, *Entropy* 16 (2014) 494-525
- [33B.2] Y. Deng, C.C. Tasan, K.G. Pradeep, H. Springer, A. Kostka, D. Raabe, Design of a twinning induced plasticity high entropy alloy, *Acta Materialia* 94 (2015) 124-133
- [33B.3] L. Liu, B. He, M. Huang, The Role of Transformation-Induced Plasticity in the Development of Advanced High Strength Steels, *Advanced Engineering Materials* article number 1701083 (2018)
- [33B.4] G. Laplanche, A. Kosta, C. Reinhart, J. Hunfeld, G. Eggeler, E.P. George, Reasons for the superior mechanical properties of medium-entropy CrCoNi compared to high-entropy CrMnFeCoNi, *Acta Materialia* 128 (2017) 292-303
- [33B.5] B. Gludovatz, A. Hohenwarter, K. Thurston, H. Bei, Z. Wu, E.P. George, R. Ritchie, Exceptional damage-tolerance of a medium-entropy alloy CrCoNi at cryogenic temperatures, *Nature Communications* article number 10602 (2016)

## 33B.6 Figures and Tables

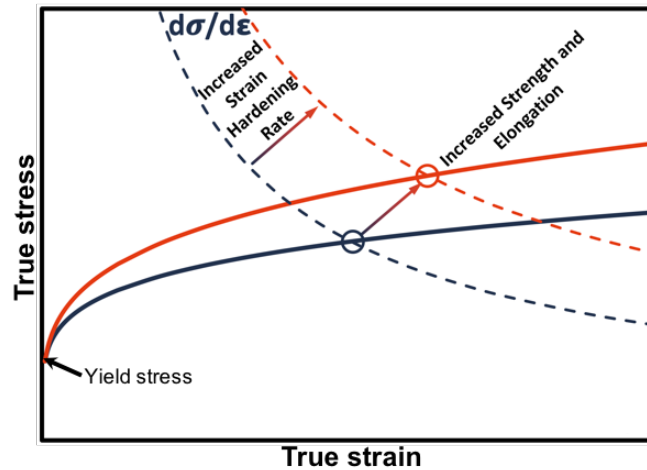


Figure 33B.1: Schematic stress strain curves for two materials with similar properties (elastic modulus, yield strength), but with different work hardening rates. Predicting the onset of necking by the instability criterion,  $\sigma = d\sigma/d\varepsilon$ , shows an increase in both ultimate tensile strength and uniform elongation associated with an increase in work hardening rate.

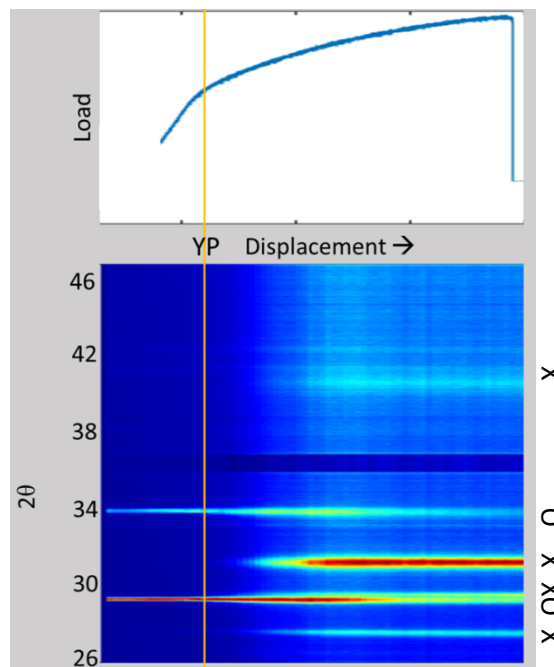


Figure 33B.2: XRD and load-displacement data for the  $\text{Co}_{0.55}\text{Cr}_{0.40}\text{Ni}_{0.05}$  alloy tested at  $60^\circ\text{C}$ , showing the evolution of HCP phase at the expense of the FCC. The transformation begins almost immediately post yield (the temporal resolution of the XRD is insufficient to determine if some small strains exist before transformation). Testing performed by Dr. Francisco Coury at the Brazilian Synchrotron Light Laboratory (LNLS) using x-rays with wavelength of  $1.033\text{\AA}$ . Peaks associated with the HCP phase are marked with an X and those associated with the FCC phase are marked with an O.

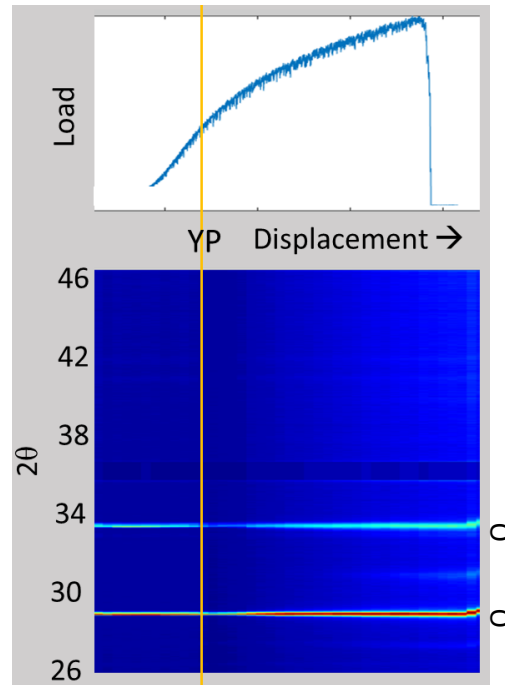


Figure 33B.3: XRD and load-displacement data for the  $\text{Co}_{0.55}\text{Cr}_{0.40}\text{Ni}_{0.05}$  alloy tested at  $600^\circ\text{C}$ , showing negligible evidence of HCP phase formation. Testing performed by Dr. Francisco Coury at LNLS using x-rays with wavelength of  $1.033\text{\AA}$ . Peaks associated with the HCP phase are marked with an X and those associated with the FCC phase are marked with an O.

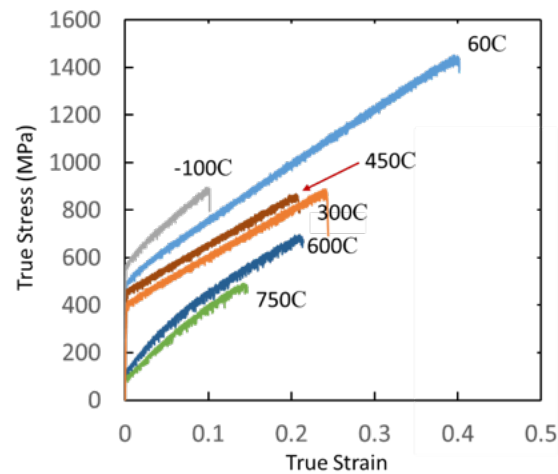


Figure 33B.4: True stress-true strain curves for the  $\text{Co}_{0.55}\text{Cr}_{0.40}\text{Ni}_{0.05}$  alloy for multiple test temperatures. Porosity from the spray forming process may have led to premature failure of the samples, as indicated by an arrow in the  $450^\circ\text{C}$  test.

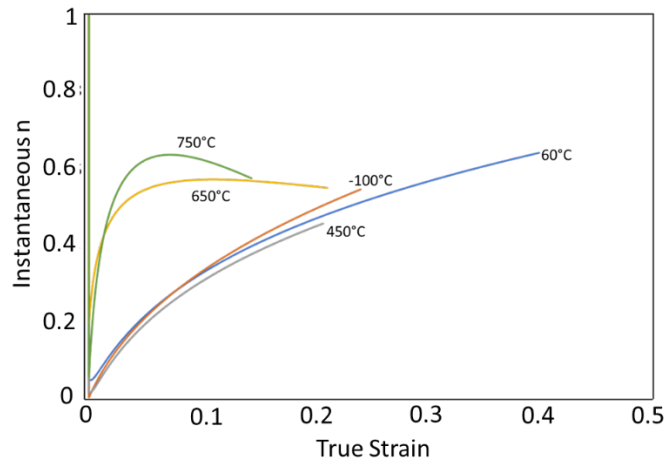


Figure 33B.5: Instantaneous work hardening exponent ( $n$ ) vs true strain ( $\epsilon$ ) plots for the  $\text{Co}_{0.55}\text{Cr}_{0.040}\text{Ni}_{0.05}$  alloy at various temperatures. The difference in  $n$  vs  $\epsilon$  behavior between low and high temperature tests suggests a difference in deformation mechanism.